#3

M EMISSION BANDS OF THE TRANSITION METALS IN THE SOLID STATE

E. MICHAEL GYORGY

TECHNICAL REPORT NO. 254

MAY 25, 1953

RESEARCH LABORATORY OF ELECTRONICS
MASSACHUSETTS INSTITUTE OF TECHNOLOGY
CAMBRIDGE, MASSACHUSETTS

The Research Laboratory of Electronics is an interdepartmental laboratory of the Department of Electrical Engineering and the Department of Physics.

The research reported in this document was made possible in part by support extended the Massachusetts Institute of Technology, Research Laboratory of Electronics, jointly by the Army Signal Corps, the Navy Department (Office of Naval Research), and the Air Force (Air Materiel Command), under Signal Corps Contract DA36-039 sc-100, Project 8-102B-0; Department of the Army Project 3-99-10-022.

MASSACHUSETTS INSTITUTE OF TECHNOLOGY

RESEARCH LABORATORY OF ELECTRONICS

Technical Report No. 254 May 25, 1953

M EMISSION BANDS OF THE TRANSITION METALS IN THE SOLID STATE

E. Michael Gyorgy

This report is based on a thesis submitted to the Department of Physics, Massachusetts Institute of Technology, June 1953, in partial fulfillment of the requirements for the degree of Doctor of Philosophy.

Abstract

The vacuum spectrograph used by R. H. Kingston for the study of the emission bands of potassium and calcium has been used, with minor modification, for the study of some of the iron group transition elements. The spectrograph employs the grazing-incidence Rowland mounting with a movable photodetector which measures the intensity of radiation in the range from 50A to 800A. The metals considered are copper, nickel, iron, manganese, and chromium. The experimental curves obtained for iron cannot, however, be considered completely satisfactory. The spectra discussed here are produced by transitions of valence electrons into the excited $3P_{3/2,\,1/2}$ states of the atom.

The experimental bands are susceptible of two interpretations. The first consists of assuming that the observed bands represent only the density of d-type electrons. The second interpretation essentially consists of assuming that an appreciable part of the experimental bands is due to the conduction electrons. This interpretation permits a plausible explanation of a number of the observed features of the bands.

M EMISSION BANDS OF THE TRANSITION METALS IN THE SOLID STATE

I. Introduction

The emission bands of the metals, iron and germanium, have been studied by a large number of authors. Beeman (1, 2, 3) and the group at Johns Hopkins have photographed the 1S emission bands of nickel, copper, and zinc. The 2P emission bands of the various metals, iron to germanium, have been obtained by Saur (4), Gwinner (5), and Farineau (6). Their results agree fairly well. The emission curves resulting from Skinner and Johnston's work (7) on the 3P bands of copper, nickel, and zinc are similar in shape to the 2P curves published by Farineau. However, for a number of reasons which subsequently will be explained, none of these results on the metals, iron to germanium, can be considered reliable.

A major difficulty in the study of soft x-ray emission bands is the exceedingly high absorption coefficient for radiation of these wavelengths, which of course, requires that the entire spectrograph be evacuated. A more serious result of the high value of the absorption is that the emitted radiation originates very near the surface of the solid which may become drastically altered by contamination. Though this problem may be somewhat alleviated by periodic evaporation of a fresh sample onto the target, it is still desirable to complete the study of the distribution of radiation intensity in as short a time as possible. In order to photograph the emission band in a reasonably short time, a relatively high power input to the target is needed. Typical values are a target current of 100 ma and 4000 volts bombarding voltage. The exposures range from fifteen minutes to several hours. Aside from the contamination difficulties caused by the long exposure time necessary with photographic plates, the high bombarding potential required produces satellite emission from the iron group metals. These satellites have obscured the structure of the emission bands from iron to germanium obtained by the aforementioned authors. To overcome these difficulties Piore suggested the use of a photomultiplier detection system to replace the photographic plate method. Piore, Harvey, Kingston, and Gyorgy (8) modified the spectrograph originally used by O'Bryan and Skinner, replacing the photographic recording system by a beryllium-copper photomultiplier built to traverse the Rowland circle mounting.

After successfully reproducing several of the curves of previous workers, Kingston received a paper by Professor Skinner giving the results he had obtained in 1939 for the iron group metals in both the 2P and 3P emission bands. The shapes of the copper, nickel, and zinc bands are similar to the curves obtained by Farineau. Since none of these curves exhibits the characteristic edge at the high-energy side of the band, and all the metals of the first two periods of the periodic table showed sharp emission edges, Kingston (9) studied the 3P emission bands of potassium and calcium, the two metals preceding the transition group, to ascertain if there was a point in the periodic table

where emission bands of metals lose the characteristic edge. He definitely established the fact that the emission edges of the metals, potassium and calcium, are sharp, as has been observed in the preceding conductors in the periodic table. On the basis of these results and the advantage of a much lower bombarding potential, it was decided to carry out a program of study on the 3P emission bands of the transition elements in the hope of obtaining similar sharp edges. The distributions of electronic-energy states in the transition elements are of particular interest, since a knowledge of them would permit a more critical examination of the magnetic properties observed.

1. Emission Process

To obtain the characteristics of the energy distribution of the conduction electrons, we study the radiation caused by the transition of an electron from the continuous band of filled valence levels into an inner atomic level. Experimentally, this means that an x-ray level of an atom is ionized by electron impact, and the intensity of the resulting radiation is studied as a function of wavelength. In principle, the inner levels are broadened into a band by the lattice potential. The broadening, however, is small compared to the experimental errors and may be neglected. Consequently, this continuous band of radiation will reflect the nature of the occupied valence levels. However, the relation between the intensity of the emitted radiation and the density of electronic levels cannot be given directly, since the radiation depends not only on the number of electrons which can make a given transition but also on the transition probability from the valence band to the excited x-ray level. It is clear that, owing to the presence of the transition probability which depends on the exact wavefunctions of the electron in the normal and excited states, the emitted radiation can be expected only to represent the distribution of electrons in the valence band in a qualitative manner. The energy spread of the emitted spectra does not depend, however, on the transition probability (unless the transition probability goes to zero) and should therefore correspond directly to the width of the occupied valence band. Unfortunately, there proves to be considerably more radiation of lower frequency than would be expected from this theory. This extra radiation is in the form of a slowly decreasing "tail" on the emission curves, making it difficult to determine the experimental width of the band. The effect of these "tails" on the long wavelength side of the band will be considered when we discuss the experimental curves.

There are two reasons why the most significant results are obtained when the emitted radiation lies in the soft x-ray region. First, it is easier to measure experimentally the intensity of radiation over a small energy band (of the order of a few volts) when the absolute energy of the radiation is small. In this case, the requirements on the experimental resolution of the spectroscope are not so stringent. The second and more cogent reason is that the natural linebreadth of a transition increases as the energy of the transition increases (10). This broadening may be said to determine the theoretical resolution, and it presents a serious limitation on the interpretation of the

work by Beeman and his group on the 1S emission curves of the iron group elements. The natural width of the 1S transition seems to be sufficiently large so that there is a great deal of blurring of the structure from this source. Some of the observed broadening of the 2P spectra (in the region 10A to 20A) presumably can be accounted for in the same way. As a result of the foregoing discussion, it is clear that the optimum resolution in the case of the iron group elements is obtained when the emitted spectrum arises from a transition into the 3S or 3P states of the atom. This is, of course, the lowest energy transition from the conduction band to a discrete inner level. The wavelength corresponding to this radiation will be between approximately 100A and 400A.

As we have stated previously, radiation of this wavelength has a high absorption coefficient and therefore is emitted near the surface of the metal. We must now consider this question in more detail to ascertain if the thickness of the layer which is effective in producing the radiation is sufficiently large so that we are assured of studying the bulk properties of the metal. Two factors determine the depth of the effective layer. The first is the absorption by the solid of the exciting electrons, and the second is the absorption by the solid of the emitted radiation. At energies of about 10,000 volts we know that electrons penetrate to the bulk of the metal and that the penetrating power of the resulting hard x-rays is much greater than the penetrating power of the electrons, so that the emitted x-rays are not appreciably reabsorbed in the metal. These results, of course, are not necessarily applicable to the energy range we are considering. Unfortunately, very little experimental work has been done along these lines with low-energy electrons and radiation. Some information on the absorption of the emitted radiation as it leaves the metal can be secured by studying the results of Skinner and Johnston (11) on the 3P absorption edges of copper and nickel. They could not determine the absolute value of the linear absorption coefficient, but they found it is of the order of 10^{-3} to 10^{-4} (A^{-1}) at the 3P absorption edge. This indicates that the emitted radiation can originate about 10^{3}A below the surface of the metal before reabsorption becomes serious, and this depth should certainly be sufficient to assure that the electronic energy states involved in the x-ray transition are not affected by the crystal boundary. No information is available on the absorption in metals of 100 to 700 ev electrons. As a result, we must infer the depth of electron penetration from our experimental results. We may do this by considering the fact that emission curves, taken at increasing values of bombarding potentials, are reproducible only after a minimum voltage is surpassed. The foregoing is interpreted as meaning that only electrons of energy higher than this minimum penetrate to the bulk of the material. However, the bombarding voltage cannot be varied over too wide a range, since at higher voltages satellites obscure the shape of the emission bands.

In addition to the previous considerations, we must also examine the possibility that variations of the absorption coefficient with energy will appreciably influence the intensity distribution of the emitted radiation. The absorption coefficient goes through a discontinuity at the $3P_{3/2}$ absorption edge. This discontinuity falls in the energy range

covered by the $3P_{1/2}$ emission band. The results of Skinner and Johnston (11) do not permit us to determine the magnitude of the discontinuity of the absorption at the $3P_{3/2}$ edge, since the $3P_{3/2}$ and $3P_{1/2}$ absorption edges are not clearly resolved. As we mentioned previously, no data of electron absorption are available. It is difficult to evaluate the result of this effect from the experimental data, since we can observe experimentally only a combination of the $3P_{1/2}$ and $3P_{3/2}$ emission bands. The largest change in the shape of the $3P_{1/2}$ emission curve caused by irregularities in the absorption coefficient would be obscured by the over-lapping $3P_{3/2}$ emission edge. Therefore, we cannot determine with any certainty whether some of the structure of the emission band is the result of reabsorption of the emitted radiation.

To simplify further discussion it will be convenient to define the spectrum notation we shall use. An x-ray line due to a transition between two inner levels will be referred to in terms of the nomenclature of these levels. For example, the line due to a transition from the $3P_{1/2}$ level to the 3S level will be referred to as the 3S, $3P_{1/2}$ line. Since states denoted by different symbols are mixed in the valence level, this nomenclature becomes cumbersome. Hence, unless it is necessary to specify a certain state in the valence band, we shall use the symbol V for the valence electrons (e.g., the $3P_{1/2}$, V-band). For convenience we shall omit the V and write just the $3P_{1/2}$ band in some cases. The $3P_{1/2}$ and the $3P_{3/2}$ levels are denoted by M_2 and M_3, respectively, in the x-ray level nomenclature. In the case of double ionization of the emitting atom which will result in a satellite emission line, the level from which the extra electron is removed will be placed in parentheses – e.g., $2P_{1/2}(3P_{1/2})3S$ satellite. An Auger transition resulting in a doubly ionized atom and a free electron will be written by separating the initial state from the two final states by a hyphen (e.g., 1S-2S, $3P_{1/2}$ Auger transition).

II. General Experimental Details

1. Experimental Equipment

Since the transition elements give a lower emission and their evaporation temperatures are higher than those of the metals previously studied with the spectrograph, it was necessary to make some modifications of the specimen chamber. A description of the spectrograph as it was used for the study of calcium and potassium is given in reference 8.

To increase the intensity of the emission, it was necessary to improve the focusing of the electron beam. The main obstacle to good focusing is the proximity of the object slit which tends to distort the electric field in the vicinity of the target. The initial attempt to improve the focusing of the electron beam was to place the target at chamber potential. With this connection extraneous radiation was observed. This radiation was attributed to photon emission produced by stray electrons striking the steel slit jaws. For this reason, the emission curves of potassium and calcium were taken with the cathode of the electron gun at the potential of the chamber. The target was at the same

potential as the deflection plates of the electron gun. This connection, however, gave insufficient intensity for the study of the transition elements.

The best focusing, without the possibility of photon emission from the slit jaws, was obtained with the cathode at ground and about 100 V between the deflection plates of the electron gun and the target, the voltage on the deflection plates being adjusted to give the desired bombardment voltage. Since the intensity of radiation is an extremely sensitive function of the bombardment voltage, all voltages were controlled by voltage regulator tubes.

The evaporation furnace was modified to make the maximum power input to the tantalum cup holding the sample to be evaporated about 80 watts. To avoid reverse emission at this power input, we use dc voltage between the cup and the cathodes. The specimen chamber was water-cooled to prevent heating of the "O" ring seals.

With the preceding arrangement we completed the study of the chromium and the copper emission bands and initiated the study of the nickel band. This work indicated the desirability of obtaining better focusing of the electron beam and a higher rate of evaporation of the sample. To accomplish these improvements a new specimen chamber was built. This new chamber is, in general, similar to the original one. The alterations consist primarily of changes in dimension to allow the installation of a larger evaporation furnace and to facilitate better focusing of the electron beam. In the new specimen chamber the target is 1.5 inches farther back along the chord of the Rowland circle connecting the object slit and the center of the grating. To give greater assurance that material evaporated from the cathode be not deposited on the target, the electron gun was placed so that the electron beam would have to be bent in a shorter radius to strike the target. The new specimen chamber has no provision for external adjustment of the slit width, since this feature was found to be unnecessary. The window for observing the target surface was also omitted, since in the original specimen chamber the glass was coated with metal after one evaporation. In any case, the target surface can be observed while the chamber is evacuated if the evaporating oven is removed and the opening is covered by a heavy glass plate. These simplifications have the advantages of decreasing the number of "O" ring seals and thereby decreasing the chance of contamination of the target surface. Mounting the electron gun on a bellows arrangement, which permits the gun structure to be moved through an angle of 10°, facilitated the focusing of the electron beam on the target. This arrangement also made it possible to compensate for errors in the construction of the gun. The gun structure itself was not changed, and the voltages on the gun electrodes and target that were used in the original specimen chamber for the study of copper and chromium gave satisfactory focusing. The space limitations the original chamber imposed upon the electron-bombardment-type evaporation furnace resulted in a comparatively fragile unit. The small spacings necessary and the structural deformations which occur at high temperature gave rise to a tendency to arc as the potential between the cathode and crucible was increased. The new chamber allows a larger and more rigid evaporation furnace with a correspondingly

higher limit on the possible bombarding voltage. Also, with more space available, it is possible to modify the evaporation furnace to meet the varying requirements of the different metals studied. The target was correctly placed with respect to the object slit and grating by means of a light beam originating at the zero-order reflection position on the Rowland circle. To check the new specimen chamber, we observed the Si 2P emission band obtained from evaporated quartz. Quartz is especially suitable for testing the spectrograph, since it contaminates more slowly than any of the other materials studied, and it is easy to extend the evaporation over a long period of time. Satisfactory curves were obtained in the first and second order.

If the contamination of the sample took place only on the target surface, any number of reproducible curves should be obtainable as long as the evaporation furnace is in continuous operation. However, this is not the case. Only a limited number of accurate curves could be obtained for each filling of the evaporating cup. The same difficulty was encountered in the study of potassium and calcium (9). Therefore, we must assume that the surface of the metal in the evaporating crucible is contaminated, probably by oxidation, as the temperature of the sample is raised. Collisions of metal and air molecules occurring in the space between the evaporating unit and the target are, of course, negligible. The oxidation of the sample in the evaporating cup makes it necessary to outgas the furnace at relatively low temperature.

A radiofrequency furnace was constructed in an attempt to improve the evaporation process (12). This type of furnace has the advantage that only the crucible holding the sample is heated, the remainder of the structure being water-cooled. As a result, the possibility of contamination of the sample by gases released from the evaporation unit is decreased. Unfortunately, the radiofrequency electric field defocuses the electron beam, making it impossible to obtain an emission curve while the evaporation furnace is in operation. As a result, any advantage in reduced contamination during the outgassing procedure is lost.

2. Background Emission

Before discussing the details of the individual emission curves, it is worthwhile to discuss some aspects of the background radiation. The most likely source of irregularity in the background is the emission of carbon lines in various orders. Carbon contamination is probable, since the diffusion pumps use organic oil. To study the effects of carbon contamination, the dependence of the 1S carbon emission band on the bombardment voltage must be determined. This dependence was investigated using a target painted with a colloidal solution of graphite and alcohol. At 1000 volts bombardment voltage, we observed the third order of the carbon emission edge at 132A. The shape of the emission band was, in general, identical with the curve obtained by Skinner (13). The intensity of the emission band was about equal to the background intensity. At 700 volts we obtained only a weak, featureless curve.

We then studied the carbon emission curve, using only contamination as a source of carbon. First we used a degreased copper target and kept the specimen chamber under vacuum for 36 hours but did not use the liquid air trap. With these conditions, and a bombardment potential of 1000 volts, we obtained the third order 1S carbon emission band, which did not, however, exhibit the sharp features of the curve obtained using the graphite-coated target. The ratio of emission to background intensity of the curve was about 20 percent. No curve could be observed at a bombardment potential of 700 volts.

Next we used a target which had been nickel-coated in the specimen chamber when the vacuum was about 1×10^{-6} mm of Hg. The liquid air trap with its exceedingly high pumping speeds for volatile organic vapors was used during the operation. Six hours after the evaporation of the nickel coat was completed, the carbon curve could not be obtained with 1000 volts.

Since all the emission curves studied were run with the liquid air trap in operation, the preceding discussion shows that emission from carbon contamination certainly did not add to the background radiation and that carbon was probably not the source of the contamination. (This subject will be discussed in a later section.) No other emission lines, such as those from material evaporated from the molybdenum thoria filaments, were observed under any operating conditions.

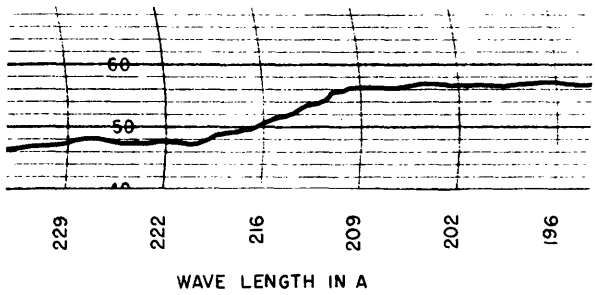

Fig. 1
Background radiation.

The only irregularities observed in the background radiation are anomalous drops in intensity at about 210A and much smaller drops around 315A and 420A. These irregularities are the second, third, and fourth order, respectively, of irregularities in the background extending from about 100A to 120A observed by Skinner (13). Skinner has shown the source of these anomalies to be almost entirely connected with absorption and dispersion of the 2p electrons of silicon in SiO_2, the main constituent of the glass of the grating. The second order is shown in Fig. 1. The curve was obtained with a copper target, 600 volts bombardment voltage, and a target current of 5 ma. The drop in intensity is about 10 counts per second. However, in this curve and in the following curves, the absolute magnitude of the background is not significant as it depends strongly on the orientation of the target, and this orientation was not exactly reproduced for all the curves studied. The effect of these irregularities on the emission curves will be discussed in the section describing the experimental curves.

III. Experimental Emission Curves

1. Copper

The observed $3P_{1/2, 3/2}$ emission band for copper is shown in Fig. 2. The sample used was the Johnson-Matthey spectrographic-grade copper rod. The rod had been vacuum cast, and as a result is oxygen-free. To fit into the tantalum evaporating cup, the sample was machined into a cylinder 1/4 inch long and 1/8 inch in diameter. The machining was done with a carbide tool. The curve shown was taken at a bombarding potential of 500 volts and a target current of 3 ma. The range shown is from 40 to 160 counts per second. The sharp emission edges at 163A and 166A correspond to the $3P_{1/2}$ and $3P_{3/2}$ emission curves, respectively. The $3P_{1/2,3/2}$ energy separation is 1.2 ev. We shall discuss the errors associated with these measurements when we summarize the results obtained for all the metals studied. The extra intensity on the short wavelength side of the $3P_{1/2}$ emission edge is attributed to satellite emission. At 600 volts bombarding potential the emission curve obtained is similar to the one shown, except that the satellite emission has increased. With 700 volts the satellites completely obscure the emission edge. Emission curves observed using 300 volts did not exhibit the sharp Fermi edge, which, as we have mentioned before, is interpreted as meaning that electrons of this energy do not penetrate to the bulk of the material. All the curves were recorded with the evaporation oven in continuous operation. No difficulties were encountered in obtaining an adhering, metallic deposit on the target.

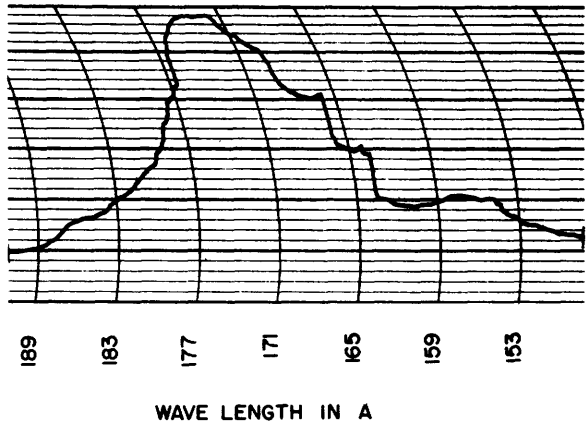

Fig. 2
Band emission curve of copper
E_b = 500 volts, I_b = 3 ma.

2. Nickel

Nickel was probably the easiest emission band to obtain, since it seemed to show the least contamination of any of the metals studied. However, since nickel alloys with tantalum, it was necessary to evaporate the sample from a graphite crucible inserted into the tantalum evaporating cup. The crucible was made from Johnson-Matthey spectrographic graphite rods. The nickel specimen was Johnson-Matthey nickel sponge. A number of emission curves were obtained from vacuum-cast nickel supplied by the National Research Corporation. These curves agreed, within the experimental error, with the emission bands obtained from the nickel sponge. The possibility of carbon contamination of the sample due to the graphite crucible was eliminated by recording some

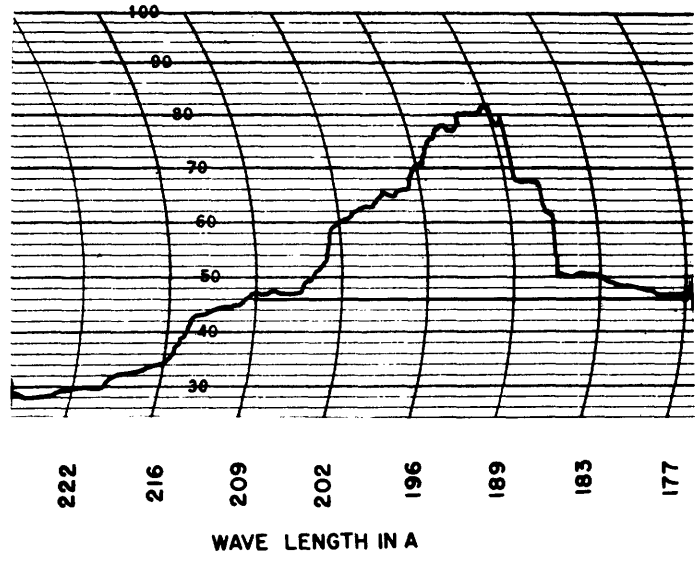

Fig. 3

Band emission curve of nickel
E_b = 500 volts, I_b = 4 ma.

emission curves, using an alumina crucible inserted into the tantalum evaporating cup. A representative emission band is shown in Fig. 3. It was recorded using a bombarding potential of 500 volts at a target current of 4 ma. The range shown is from 50 to 200 counts per second. Unfortunately, the long wavelength side of the emission band is near the region of background irregularity discussed earlier. A comparison of the nickel emission band and the continuous spectrum shown in Fig. 1 makes it clear that the anomaly in the background is only appreciable at wavelengths larger than 209A. As a result, we may assume that the background radiation is at the level indicated on the experimental curve. The emission band then ends at about 206A. To keep any contamination effects to a minimum, it is desirable to record the curves as rapidly as possible. The emission edges were therefore taken in a shorter time than was consistent with the response time of the counting-rate meter. As a result, the kinks in the $3P_{1/2, 3/2}$ edges are due to the response time of the counting-rate meter and are not real. On curves where we only observed the high-energy side, the inflections do not occur. The emission curve shows satellites similar to the ones obtained for copper. In Fig. 4 it can be seen how the satellite intensity increases relative to the $3P_{1/2, 3/2}$ V-band intensity as the bombarding potential is increased. To obtain these curves the target current was carefully adjusted to make the background emission of the three curves equal. The curves were observed using the 200 counts-per-second scale of the counting-rate meter and 500, 600, and 700 volts bombarding potential. The respective target currents used were 4, 3, and 2.5 ma. As we have stated earlier, the absolute intensity of the emission bands cannot be related to the target current and bombarding voltage, since the position of the focus of the electron beam on the target is not exactly reproducible.

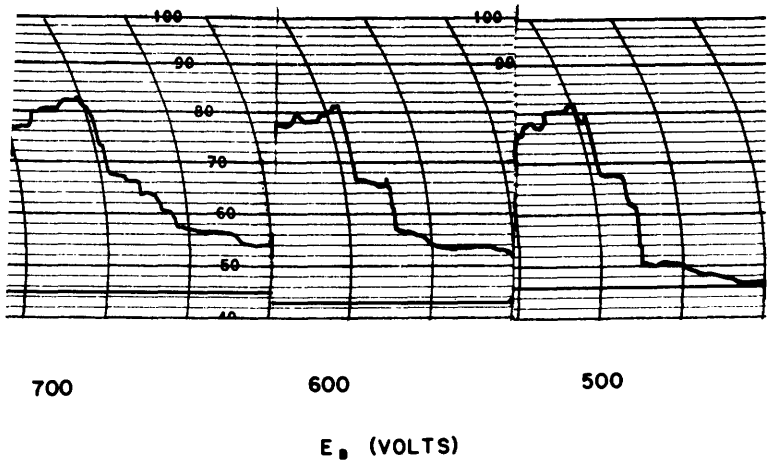

Fig. 4

Emission edges of nickel (the background level is indicated for each curve).

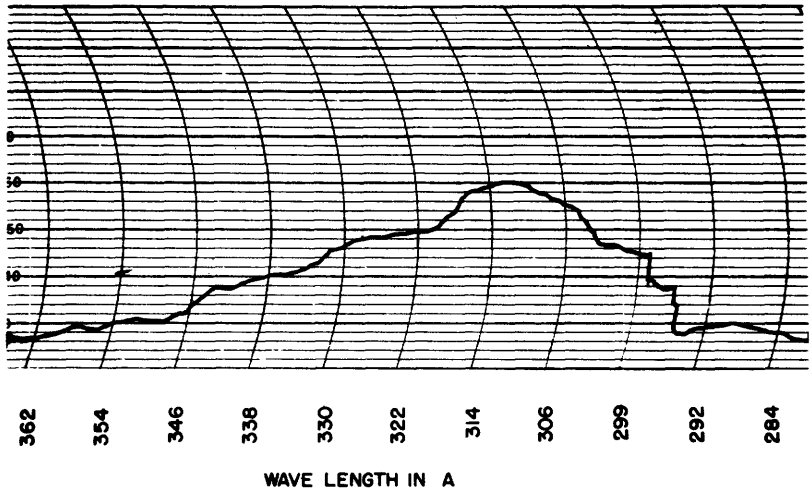

Fig. 5

Band emission curve of chromium
E_b = 600 volts, I_b = 3 ma.

3. Chromium

The emission band of chromium was considerably more difficult to obtain as a result of the contamination of the sample. Chromium is evaporated onto the target at a temperature below the melting point. In fact, it was impossible to raise the temperature sufficiently high to melt the sample. For the study of the calcium emission band (9) the metal was also evaporated from the solid state and Kingston attributes the added contamination difficulties to an oxidized layer formed on the surface of the solid calcium, preventing metal atoms from leaving the material. Presumably, there is sufficient agitation in a molten metal to break through any oxide layer on the surface. It is, however, impossible to make any definite statements about the relative rates of contamination, since it is not certain that the same percentage of oxidation will produce equal effects on the emission curves of different elements. The experimental curve is shown in Fig. 5. This curve, as in the case of all the emission bands studied, was taken with the evaporation furnace running during the observation time. The sample used to obtain the curve was the Johnson-Matthey spectrographic-grade electrolytic chromium. In earlier attempts with a commercial-grade electrolytic chromium, only a very weak, featureless curve could be obtained. The bombarding voltage was 600 volts, and the target current was 3 ma, which resulted in a maximum intensity of the band of about 60 counts per second. In contrast to the case of copper and nickel, the bombarding potential used was sufficient to ionize the 2P level. Whenever possible, it is desirable to eliminate any extra background emission which may be produced by the excitation of higher-energy states.

A curve of contaminated chromium is shown in Fig. 6. This curve was obtained about ten minutes after the evaporation had been started. Although the furnace was in continuous operation, depositing new sample on the target, sufficient contamination must have taken place in the evaporating crucible to produce an appreciable percentage of

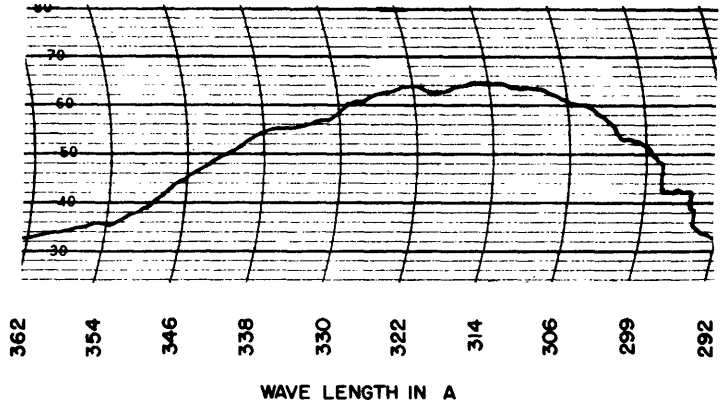

Fig. 6

Band emission curve of contaminated chromium
E_b = 600 volts, I_b = 5 ma.

impurities on the target surface. The curve shown was taken at 600 volts and a target current of 5 ma. A curve taken about 15 minutes after the evaporation furnace is turned on no longer shows the sharp Fermi edge. By noting the change that the impurities have produced in the shape of the emission band, especially between 314A and 322A, we may infer that the structure of the observed curve is not appreciably affected by the third order of the background irregularity. This viewpoint is also supported by the fact that the background level is constant from the high wavelength side to the low wavelength side of the chromium emission curve. The parts of the nickel curve attributed to the anomalies in the continuous spectrum are, of course, not affected by the contamination of the nickel.

4. Manganese

Even though manganese is evaporated from the molten state, the manganese emission band was more difficult to obtain than the chromium band. This may be at least partially explained by noting that pure electrolytic manganese is extremely active chemically, and it very rapidly becomes covered with a thin film of oxide. The difficulties caused by contamination could not be alleviated by a higher rate of evaporation, since this resulted in a somewhat spongy and nonadherent deposit on the target. An attempt to improve the rate of evaporation and still obtain a metallic deposit was made by doubling the diameter of the evaporating cup and using a slightly smaller power input. This modification gave no observable change of the emission band. The first sample we tried to use was the Johnson-Matthey electrolytic manganese. Since this sample was supplied in thin plates, the surface layer of oxide was a relatively large fraction of the total material. As a result, evaporation of this sample did not give a pure deposit of metal on the target surface. The sample used to obtain the curve shown in Fig. 7 was

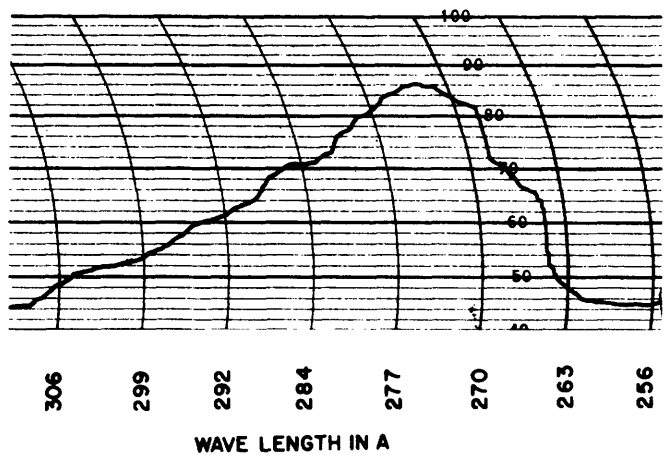

Fig. 7

Band emission curve of manganese
E_b = 600 volts, I_b = 6 ma.

98.6 percent electrolytic manganese; the major impurity was 0.9 percent iron. To expose as much fresh surface as possible and to obtain a convenient size, the metal particles were ground by means of a mortar and pestle before being placed in the tantalum cup. The low intensity made it necessary to use the 100 counts-per-second scale of the counting-rate meter. The range shown is from 40 to 100 counts per second. The curve was recorded with a bombarding voltage of 600 volts and a target current of 6 ma. The larger response time corresponding to the 100 counts-per-second scale and the more rapid contamination of the sample made it impossible to obtain curves that were reproducible with the accuracy obtained for the copper, nickel, and chromium curves.

5. Iron

It was impossible to obtain a satisfactory iron emission band. The intensity and the ratio of intensity to background are very low. The very rapid contamination of the sample made it imperative to record the curves rapidly. The required higher speed of transversal resulted in more pronounced kinks in the emission edges. However, since the observed curves show more structure than those previously obtained, it is probably worthwhile to consider them.

The sample used to obtain the curve shown in Fig. 8 was Johnson-Matthey spectrographic-grade iron sponge. Similar curves were obtained with vacuum-cast iron supplied by the National Research Corporation. The samples were evaporated in an alumina crucible fitted into the tantalum cup, or in some cases, an alumina crucible with the outside coated with colloidal carbon. The latter arrangement eliminated the troublesome failures of the tantalum cup occurring at high temperatures, making a higher power input to the crucible possible. The higher potential between the cathode and the crucible of the evaporation unit tended to defocus the electron beam striking the target. An attempt to alleviate this difficulty by screening the evaporation furnace was not successful, and consequently, it was necessary to realign the electron gun to compensate

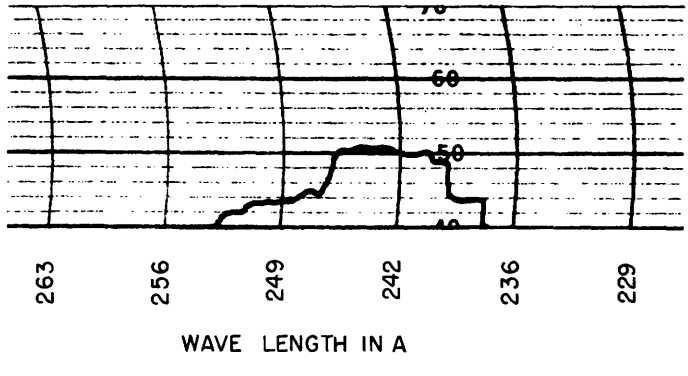

Fig. 8

Band emission curve of iron
E_b = 700 volts, I_b = 6 ma.

for the defocusing. The new alignment was checked by observing the Si 2P emission band obtained from evaporated quartz. This trial was carried out under the same experimental conditions as those required for the observation of the iron emission band.

The iron curves were recorded using the 100 counts-per-second scale and a target current of 6 ma at 700 volts bombarding potential.

We did not attempt to study the emission band of cobalt, since this band is in the region of the second order of the anomalous background. Under these conditions any interpretation of the band shape would be very uncertain.

6. Emission Edges

One feature of the observed emission bands which is independent of the transition probabilities is the position of the sharp Fermi edge. The edges, corresponding to the $3P_{1/2}$ and $3P_{3/2}$ emission bands, are clearly shown on the preceding experimental curves. The absolute energies of these edges are, of course, the $3P_{3/2}$ and $3P_{1/2}$ ionization potentials which can be derived from ordinary x-ray spectra. The hard x-ray spectrum does not, however, resolve the $3P_{3/2,1/2}$ separation. In Table I we compare the position of the observed edges with the ionization potentials given by Sanner. These results are quoted in a review article by Niehrs (14). The new values for the ionization potentials are in better agreement with the position of the observed emission edges than are the values given by Siegbahn (15).

Table I

Energy of the $3P_{1/2}$ Edge

	Observed (ev)	X-ray Value (ev)	Mean Absorption Edge (ev)	$3P_{1/2}$ Absorption Edge (ev)
Chromium	42.1 ± .2	42.2		
Manganese	46.8 ± .2	47.3		
Iron	52.3 ± .2	53.4		
Nickel	66.7 ± .2	67.2	65.5	67.7
Copper	75.9 ± .2	75.9	74.0	77.3

For example, Siegbahn gives the $3P_{3/2,1/2}$ ionization potential of nickel as 73.1 ev, 6.4 ev higher than the observed value. It should be emphasized that the deviations given for the observed energy are a reasonable limit on the error and are not the probable error. The reasonable limit is determined by considering possible inaccuracies in the calibration of the spectrograph. The agreement is surprisingly good, since the x-ray values involve an accurate fixing of the 1S absorption edge.

From the theory of metals we know that the $3P_{3/2,1/2}$ absorption edges should coincide with the corresponding emission edges. In column 3 of Table I we give the

values of the absorption edges obtained by Skinner and Johnston (11). Since the edges are diffuse and the $3P_{3/2,1/2}$ separation is not clearly resolved, the value given in the table is a mean energy defined by the foregoing authors as that at which the extra absorption is half the total extra absorption. However, Skinner in a private communication states that contrary to the statement in the article, the edges are resolved. This new value of the $3P_{1/2}$ edge is given in column 4 of Table I.

In Table II we give the observed $3P_{3/2,1/2}$ separation and the separation obtained by Skinner from the reinterpretation of the absorption curves mentioned above.

As in Table I, the indicated deviations are a reasonable limit on the error. The agreement is not good, but since Skinner does not give a discussion of the accuracy of his data, it is impossible to comment on the discrepancies between the values obtained from the absorption curves and those obtained from the observed emission curves. It may be noted, however, that the differences are mainly due to the fixing of the $3P_{1/2}$ edges. The positions of the $3P_{3/2}$ edges agree fairly well. The observed positions for copper and nickel are 74.7 ev and 65.8 ev; the values given by Skinner are 74.3 ev and 65.4 ev, respectively.

Table II

$3P_{3/2,1/2}$ Separation

	Observed	According to Skinner
Chromium	0.45 ± .1	
Manganese	0.6 ± .1	
Iron	0.6 ± .1	
Nickel	0.9 ± .1	2.3
Copper	1.2 ± .1	3.0

7. Satellites

The observed satellites are the result of double ionization of the emitting atom. Since the probability of direct double ionization by electron impact is negligible, the double ionization must be the result of a radiationless Auger transition. The importance of these radiationless transitions in the interpretation of hard x-ray spectra was first pointed out by Coster and Kronig (16). The Auger effect also plays an important part in the understanding of the observed intensities of the $2P_{3/2,1/2}$ spectra of such metals as Na, Mg, and Al (13). In metals there is generally no difficulty in finding a final state for which an Auger transition of the type $nS\text{-}nP_{1/2}$, V is energetically possible. Even though the $nP_{3/2,1/2}$ energy separation is small, Auger transitions such as $nP_{1/2}\text{-}nP_{3/2}$, V are possible, since the electron can be emitted into the continuum of unoccupied levels just above the conduction band. In fact, as Skinner was unable to detect the 2S emission band, we must assume that the $2S\text{-}2P_{3/2,1/2}$, V Auger transition probability is greater than the probability of 2S, V radiative transition. The Auger transition shortens the

lifetime of the 2S excited state so that the 2S absorption edges are very broad. Similar radiationless transitions explain the anomalies in the intensities of the $2P_{3/2}$ and $2P_{1/2}$ emission bands. Statistically, the relative intensity of the $2P_{3/2}$ to the $2P_{1/2}$ emission band should be 2. The observed values are given by Skinner as 20 for manganese and 9 for aluminum. Skinner accounts for the differences by assuming a $2P_{1/2}$-$2P_{3/2}$, V Auger effect which diminishes the probability of the $2P_{1/2}$, V radiative transition. Unlike the case of the 2S band, the $2P_{1/2}$ band, though weak, can be observed. Therefore, we would not expect the $2P_{1/2}$ absorption edge to be appreciably broadened. This is, in fact, the case. In view of the introductory statements, we would expect an atom in a doubly ionized state such as $2P_{3/2}$, V to give rise to satellite emission. We have, however, neglected one further condition for satellite emission (17): the radiation must be emitted before the vacancy in the conduction band has passed from the excited atom over to a neighboring atom. The absence of satellites in the spectra of sodium, magnesium, and aluminum shows that for these metals this extra condition is not fulfilled.

Energy considerations require that the extra ionization causing the observed satellite of the $3P_{3/2,\,1/2}$ emission bands of the transition elements must be in the valence band. (By valence band we mean the energy band derived from the 4s, 4p, 3d and higher levels.) This shows that the second condition for satellite emission discussed in the preceding paragraph is fulfilled. That is, the radiation is emitted before the vacancy in the valence band has passed from the excited atom. The difference in this respect between magnesium and aluminum and the transition elements is probably due to the more tightly bound 3d-bands. Since the s-p band of the iron group elements is presumably responsible for most of the electrical conductivity, we may assume that vacancies in this band behave in a fashion similar to vacancies in the s-p band of aluminum and do not give rise to satellite emission. Then the satellites must result from an emitting atom with the $3P_{3/2,\,1/2}$ and 3d level excited. These double ionizations are, of course, the result of the $3S\text{-}3P_{3/2,\,1/2}3d$ radiationless Auger transition. We write $3S\text{-}3P_{3/2,\,1/2}3d$ instead of $3S\text{-}3P_{3/2,\,1/2}$, V since we want to specify a certain type of band. As stated above, the $3S\text{-}3P_{3/2,\,1/2}$, 4s Auger transition would result in an increase of the $3P_{3/2,\,1/2}$ intensity but would not result in satellite emission. Auger transitions of this general type are to be expected since the 3S, V and 3S, $3P_{3/2,\,1/2}$ radiative transitions could not be observed. The increase of the $3P_{3/2,\,1/2}$(3d) V satellite intensity (Fig. 4) with increasing voltage is consistent with the expected increase of the 3S ionization cross section. But owing to the complicated nature of the process occurring at the x-ray target, it is not possible to make any quantitative statements about the way the cross section for inner-shell ionization varies with electron energy. The Auger effects discussed should shorten the lifetime of the excited 3S state. Therefore, the 3S absorption edge should be broadened, but it should not, of course, be weak. Unfortunately, Skinner could not observe the broadened 3S absorption edge for copper and nickel, so we are unable to make any comparisons with the width of the 2S absorption edge of aluminum.

The absence of the 3S, V emission band and the 3S, $3P_{3/2,\,1/2}$ line was only certainly established for nickel. The wavelength of the copper 3S emission band in the first order is not in a suitable range and the absence of the second order is hard to determine, since the expected intensities would necessarily be low. The probable wavelengths of these bands were derived from the hard x-ray data (14). The rapid contamination of the other metals studied made a systematic search for the 3S emission band impossible. However, we can say with relative certainty that if the nickel 3S, V-band or the 3S, $3P_{3/2,\,1/2}$ line exists, their intensities are less than 10 percent of the intensity of the $3P_{3/2,\,1/2}$ band. We shall assume that the case of nickel is representative of all the metals studied.

As in the case of aluminum and magnesium, the anomalies in the intensity of the $3P_{1/2}$ and $3P_{3/2}$ emission bands can be explained by assuming certain Auger transitions. The observed ratio of the $3P_{3/2}$ to the $3P_{1/2}$ intensities is about one-half. Statistically, the ratio should be 2. The difference can most simply, but of course not uniquely, be explained by postulating that the probability of the $3P_{3/2}$ - V, V Auger transition is larger than the probability of the $3P_{1/2}$ - V, V transition. Neither transition probability, as may be seen on the experimental curves, is so large as appreciably to broaden the observed emission edges.

IV. Electron Distribution

1. Relation of Emission Curve to Electron Distribution Function

To analyze the experimental curves let us follow the procedure given by Mott, Jones, and Skinner (18). We denote the number of electrons per unit energy range by dN/dE and the optical transition probability from a state with energy E to the 3P level by f(E). For convenience we measure E from the bottom of the valence band. Then the intensity of the emission band, measured as number of quanta per second in the range E to E + dE is given by $I(E) = f(E)\, dN/dE$. The 3P level in the metals studied has wavefunctions practically confined to a region around individual nuclei, small compared with the lattice constant of the metal. For example, in the case of copper the ratio of the radius of the 3P function to the lattice constant is roughly equal to 1/10 (19). Consequently, the transition probability f(E) is influenced only by those parts of the valence electron wavefunction which lie in the neighborhood of the nuclei. In this region the valence electron wavefunctions may be approximated by atomic wavefunctions. So ψ_{nk}, the wavefunction of a lattice electron, may be written as

$$\psi_{nk} = a_s^n(k)\psi_{4s} + a_p^n(k)\psi_{4p} + a_d^n(k)\psi_{3d} + \ldots$$

$$a_s^n(k)^2 + a_p^n(k)^2 + a_d^n(k)^2 + \ldots = 1$$

where ψ_{4s}, ψ_{4p}, etc., are the free atomic wavefunctions and k is the wave vector denoting the state of the electron. The subscript n refers to the s-p band and the

five d-bands. We regard

$$a_s^n(k)^2(dN/dE)^n \quad \text{and} \quad a_p^n(k)^2(dN/dE)^n$$

as the numbers of the s and p type electrons, respectively, corresponding to k in the n^{th} band. Then we have

$$(dN/dE)_s^n = a_s^n(k)^2(dN/dE)^n \quad \text{and} \quad (dN/dE)^n = \sum_i (dN/dE)_i^n$$

As a result

$$I(E) = f(E)\, dN/dE$$

becomes

$$I_n(E) = \nu^2\left\{f_{sp}(dN/dE)_s^n + f_{dp}(dN/dE)_d^n\right\}$$

where

$I_n(E)$ is the intensity of the n^{th} band; $(f_{sp})^{1/2}$ and $(f_{dp})^{1/2}$ are analogues to atomic transition dipole moments and may now to a first approximation be regarded as independent of the energy for at least a small range of E. The frequency of the emitted radiation is ν. The observed intensity is, of course, equal to the sum of the intensities from the six bands, so

$$I(E) = \nu^2 \sum_n \left\{f_{sp}(dN/dE)_s^n + f_{dp}(dN/dE)_d^n\right\}$$

One more modification of the observed intensity must be made. The photomultiplier of the spectroscope observed $I(\lambda)$. So the relation of the observed intensity to electron distribution is given by $I(\lambda) = \nu^2 I(E)$. To obtain the distribution function of p-type electrons, it would be necessary to study a transition to an s state.

In the same paper (18) Mott, Jones, and Skinner use the method of Bloch waves to calculate the behavior of a_i in the s-p band. Specifically, they treat the case of an atom with an S-ground state and with a P state of slightly higher energy. They find that a_p increases from zero to one and that, for small k, a_p is proportional to k. The results are obtained for a simple cubic lattice, but the authors state that the results may be expected to apply to more complicated structures. In fact, this behavior of a_i qualitatively fits the experimental data of such metals in the first and second period of the periodic table as magnesium and beryllium where the energy separation of the s and p states is less than the width of their filled valence bands. The iron group transition elements are more complicated in this respect, since the bands derived from the 4s, 4p and 3d states overlap. Not much of a general nature can be said of the relative positions of the s-p and d-bands, and each case must be examined individually. The most complete theoretical discussions of this problem make use of the cellular method introduced by Wigner and Seitz and extended by Slater. To date, the energy bands of copper,

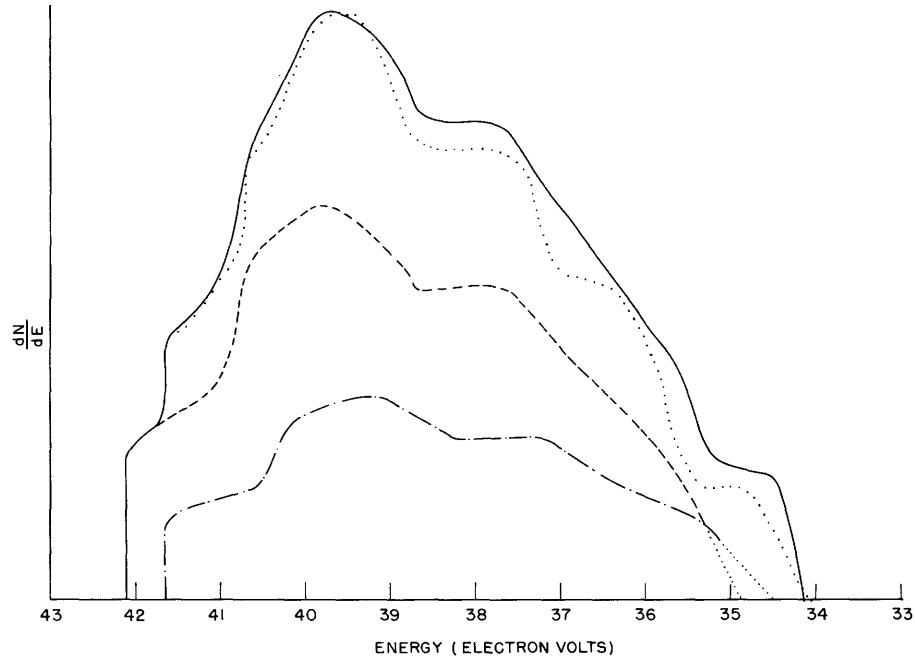

Fig. 9
Electron distribution in chromium.

nickel, and iron have been calculated by this method (20,21, 22, 23). We shall consider the results of these calculations in a later section.

2. Electron Distribution of Chromium

The experimental curves are modified to represent the distribution of the s-type and d-type electrons by the method just outlined. The background of the experimental curves is eliminated. Then, to minimize the effect of fluctuations, we average the observed intensities. The average intensity with the ordinate divided by a factor proportional to the fourth power of the absolute energy is plotted as a function of energy (Fig. 9). This curve is a superposition of the modified $3P_{3/2}$ and $3P_{1/2}$ emission bands. For simplicity the emission edge has been sharpened and, of course, the structure due to the response time of the counting-rate meter has been neglected. The modified experimental curve (Fig. 5) has been added (dotted) for comparison.

In order to disentangle the $3P_{3/2}$ and $3P_{1/2}$ bands, the relative intensities of these bands must be known. Fortunately, the satellites are effectively clear of the emission band in the case of chromium, and therefore the ratio of $3P_{3/2}$ and $3P_{1/2}$ intensities is given unambiguously by the magnitude of the respective emission edges. The average value obtained for this ratio is $0.52 \pm .04$. With the assumption that the two overlapping bands have identical structure, we are then able to separate the bands by graphical means. No theoretical justification for this assumption can be given; nevertheless, it is the only feasible one to make. The resulting $3P_{3/2}$ and $3P_{1/2}$ curves, representing

the sum of the s-like and d-like electron densities weighted by the appropriate transition probability, have been added to Fig. 9. The low-energy side of the experimental curve is not reliable, and this part of the curve is emphasized by the ν^4 factor. Therefore, the bands were completed by the dotted lines at the low-energy end, showing the probable position of the bottom of the Brillouin zone. The method of separation essentially consists of extending the $3P_{3/2}$ and $3P_{1/2}$ curves back toward the low-energy side in increments equal to the $3P_{3/2,1/2}$ energy separation. Since this method will in general not give a smooth curve, but rather an oscillatory curve with a period of twice the $3P_{3/2,1/2}$ separation, the smooth curve we obtain gives us some confidence in our experimental curves.

3. Electron Distribution of Nickel

The superposition of the modified $3P_{3/2}$ and $3P_{1/2}$ curves shown in Fig. 10 is obtained by the same method that was used for chromium. The modified experimental curve (Fig. 3) taken at 500 volts bombarding potential is added (dotted) for comparison.

As the satellites are not clear of the main emission band, we must examine the problem of finding the correct intensity ratio of the two emission bands in more detail. We have already stated that the shape of the experimental curve on the long wavelength side of the $3P_{1/2}$ emission edge is not altered as the satellite intensity is increased. In fact, the majority of the experimental curves used to obtain the average intensity, from which the modified distribution curve given above is derived, was taken at 600 volts bombarding voltage. The curves showed the expected larger relative satellite intensity (cf., Fig. 4). On the basis of these observations we may then assume that the shape of the emission curve would be unchanged if the satellite intensity could be reduced to zero. In other words, to find the correct ratio of the $3P_{3/2}$ to the $3P_{1/2}$ intensity,

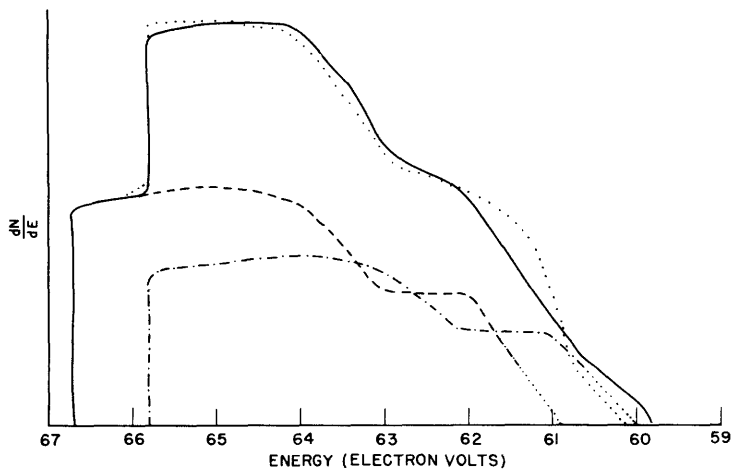

Fig. 10
Electron distribution in nickel.

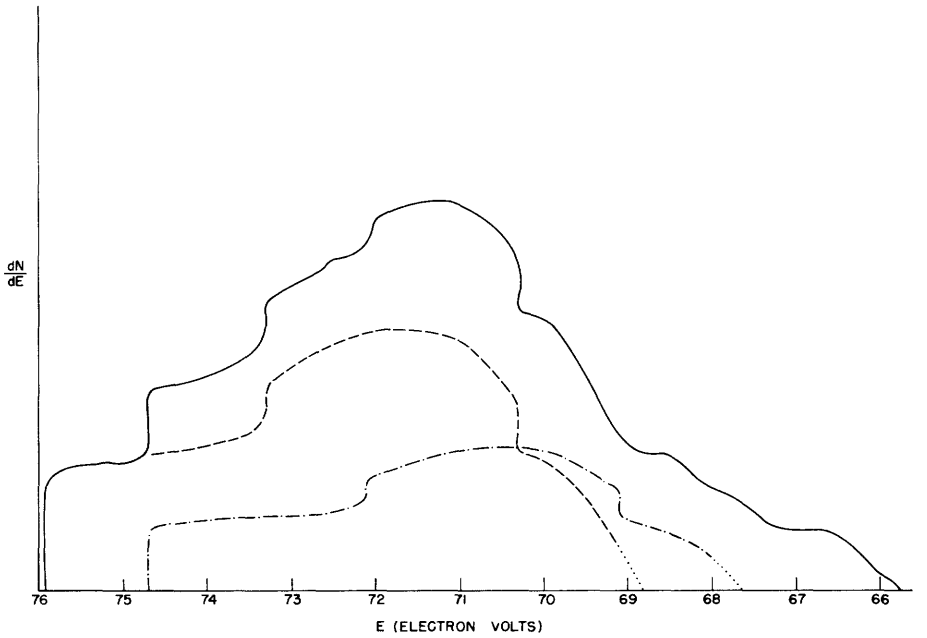

Fig. 11
Electron distribution in copper.

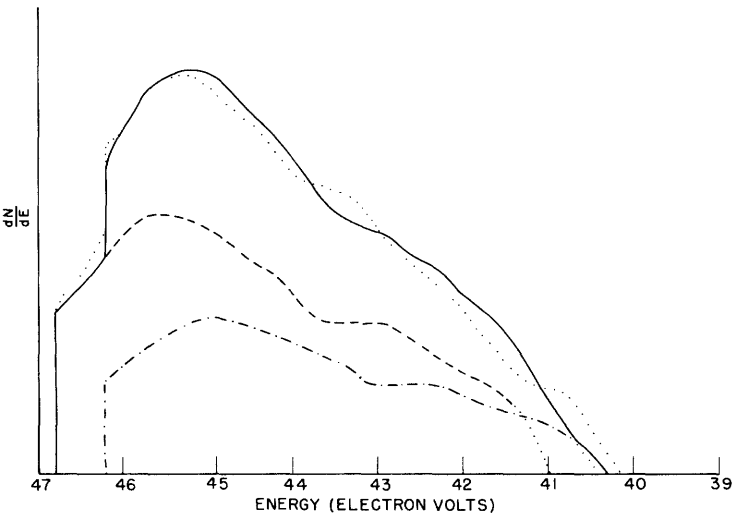

Fig. 12
Electron distribution in manganese.

the $3P_{1/2}$ emission edge must be measured from the level of the background. With this interpretation the average value of the $3P_{3/2,1/2}$ intensity ratio is $0.71 \pm .05$. The two bands can then be separated as indicated. The doubtful low-energy parts of the curves are dotted.

4. Electron Distribution of Copper

The modified curve obtained from the experimental curve shown in Fig. 2 is given in Fig. 11.

The experimental observations concerning the shape of the copper emission band and the intensity of the satellite emission were the same as those of nickel. Therefore, we again assume that the structure of the emission band would be unchanged if the satellite intensity could be reduced to zero. The ratio of the $3P_{3/2}$ to the $3P_{1/2}$ intensity then is $0.51 \pm .03$. This ratio is verified by the relative magnitude of the inflections of the modified curve at 73.3 ev and 72.1 ev. Unfortunately, the expected drop at 69.1 ev corresponding to the observed drop at 70.3 ev is obscured by the inherent inaccuracies of the low-energy part of the curve.

5. Electron Distribution of Manganese

No new features were encountered in obtaining the electron distribution of manganese, shown in Fig. 12. The curve was obtained from an average of experimental emission bands. The curve shown in Fig. 7 is given (dotted) for comparison. The ratio of the $3P_{3/2}$ to the $3P_{1/2}$ intensity is $0.58 \pm .08$.

6. Electron Distribution of Iron

The distribution curve obtained from the average of experimental curves is shown in Fig. 13. Considering the low accuracy of the experimental bands, we would not expect the details of this curve to be meaningful. In fact, below 50 volts the method of separation caused the separated curves to be somewhat oscillatory. For the sake of clarity we have drawn a smooth curve, but in no case was the ordinate changed by more than 10 percent. The distribution derived from the experimental curve shown in Fig. 8 is added (dotted) for comparison. The fair agreement of this curve with the curve calculated from the average intensities gives us some confidence in the general outline of the electron distribution obtained. The low intensities of the emission bands made it impossible to obtain an accurate value of the $3P_{3/2,1/2}$ intensity ratio. The average value of this ratio is $0.53 \pm .11$.

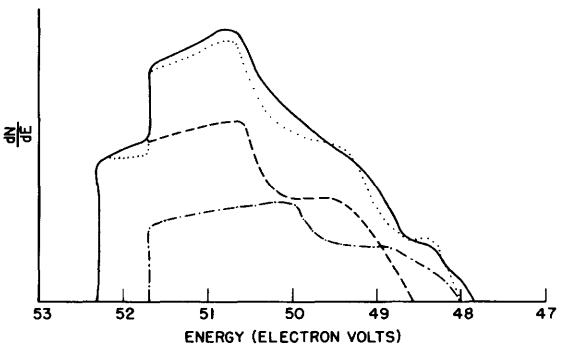

Fig. 13
Electron distribution in iron.

7. Emission Bandwidth

To obtain the width of the $3P_{3/2}$ and $3P_{1/2}$ bands, we must obviously use the separated curves derived in the preceding sections. The accuracy of the values found for the bandwidths depends to some extent upon the correctness of the assumptions used to disentangle the superimposed curves. In addition, the inherent low accuracy of the long wavelength side of the experimental curves precludes the possibility of giving a definite value for the low-energy limit of the band. Therefore, the deviations given for the observed bandwidths are an estimate of the accuracy of the values obtained and are not the probable error. In Table III we compare the observed results with the results obtained by Skinner. The latter values are taken from the Skinner manuscript referred to in the introduction. To obtain the values given in the table, Skinner defines the bandwidth of his experimental curves as follows: the high-energy end is taken as the midpoint of the presumed edge; the other limit is found by projecting the straight part of the band on the low-energy side of the maximum to the axis.

Table III

Emission Bandwidth

	Observed (ev)	According to Skinner (ev)	
	$^3P_{3/2}$	$^3P_{3/2}$	$^2P_{3/2}$
Chromium	7.2 ± 1.0	6.3	6.3
Manganese	5.8 ± 1.0	6.0	5.7
Iron	3.7 ± 1.0	4.4	5.0
Nickel	5.8 ± 0.5	4.7	5.0
Copper	7.1 ± 0.5	7.0	6.7

As we have stated previously, part of the uncertainty concerning the interpretation of the intensity on the long wavelength side of the emission bands is due to the presence of "tails" on the emission curves. Seitz (24) suggests that the "tails" are the result of transitions from one of the discrete, or excitation, levels lying below the valence band. The discrete levels are the result of the Coulomb-like potential that the atom ionized in one of the inner shells introduces into the lattice. Slater points out that these levels are analogous to the discrete levels produced by N-type impurities in a semiconductor (25). Skinner (13) accounts for the low-energy "tails" by assuming that the lifetime of the state in which there is a vacancy in the valence band is sufficiently short to broaden the level appreciably. The lifetime of a vacancy in a level is of course determined by the probability that an electron higher in the band may make a transition into the vacancy. (Radiative transitions are in general not allowed.) This probability will be low for a vacancy near the top of the occupied levels, and consequently, the emission edge would not be broadened.

V. Discussion of the Experimental Data

In order to discuss the experimental data, it is convenient to review first some simple consequences of the band theory applied to the transition elements. Mott (26) first proposed the band model employing a wide low-density s-p band capable of holding 2 electrons per atom and a rather narrow d-band capable of holding 10 electrons per atom. The d-band would be expected to be narrow because the 3d electrons are largely confined to the neighborhood of the atomic nuclei and consequently less affected by neighboring atoms. The small energy separation of the atomic 4p, 3d and 4s levels indicates that at the actual internuclear distance the d-band and s-p band overlap. In fact, to account for the high-electronic specific heat and the observed saturation magnetization, it is necessary to assume that for nickel, copper, and iron the partly filled s-p and d-bands are occupied to the same level. For copper the Fermi level is above the d-band. With the postulate that for the ferromagnetic metals the d states of one kind of electron spin are completely filled, we can find the number of holes in the 3d-band and the number of electrons in the s-p band from the measured saturation magnetization. The number of electrons in the s-p band then is 0.6 and 0.22 for nickel and iron, respectively. The general features of the energy bands we have briefly outlined are verified by the calculation of Slater (21, 27) for copper and nickel.

For the reasons given above, the density of states having d-like symmetry around the individual atoms of the lattice is presumably higher than the density of states having s-like symmetry. Also, at any rate for hydrogen-like wavefunctions, the 3d, 3p transition has a greater probability than the 4s, 3p transition. Hence, we might expect that the observed emission band represents only the five d-bands. With this interpretation we can compare the observed electron distribution with the d-bands calculated for the transition elements.

The energy bands of copper have been calculated by Slater (21, 27) from an extension of Krutter's work on copper (28). The electron distribution obtained by Slater is shown in Fig. 14. The width of the double-peaked d-band is about 5.5 ev. The filled electron levels in the overlapping 4s-band, which we are neglecting for the present, extend about 2 ev beyond the limit of the filled 3d-band. Krutter's calculations were carried out by the cellular, or Wigner-Seitz method.

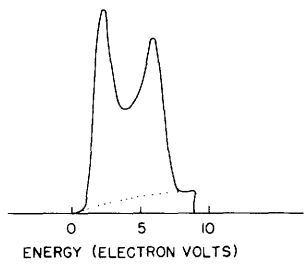

Fig. 14
Calculated electron distribution of copper (after Slater).

Slater (21) extrapolates to the preceding elements from the energy bands calculated for copper. The extrapolation rests upon the assumption that the energy bands remain the same for the preceding transition elements and that only

the height to which they are filled is changed. The height to which the levels are filled is, of course, determined by the number of electrons to be accommodated. The extrapolation to nickel can be made with some assurance, since nickel has the same face-centered-cubic crystal structure as copper. The electron distribution for nickel is then the same as shown in Fig. 14 but with the Fermi edge roughly in the middle of the high-energy peak. It should be emphasized that the structure of the calculated band cannot be compared directly with the structure of the observed band, since the observed band reflects only the density of the s-type and d-type electrons weighted by the appropriate transition probabilities. It is doubtful, however, if the transition probability can account for the fact that the considerable concentration of states near the bottom of the calculated d-band is not observed in the experimental nickel emission band. But for the following reason we shall not concern ourselves with such discrepancies in the observed and calculated shapes of the emission bands: The details of the structure of the energy bands depend upon the exact nature of the wavefunctions, so we would not expect the shape of the bands to be as accurate as the pertinent energy values. Therefore, we shall restrict ourselves here to comparing the energy spread of the electron distributions. The widths of the d-bands obtained by Slater are given in column 2 of Table IV. Since the calculated s-p band does not extend below the low-energy limit of the d-band, the widths of the calculated d-bands are, except in the case of copper, equal to the total width of the energy band.

The validity of the extrapolation discussed in the preceding paragraph can be estimated from the later work of Manning (22) on the energy bands of body-centered iron. These calculations were carried out by the cellular method. The width of the calculated electron distribution, and for the reasons given above, the width of the d-band, is 5 ev or 5.5 ev depending upon how much weight is given to the low-energy portion of the distribution curve. This value is not in poor agreement with the width of 4.3 ev obtained by Slater. Furthermore, the structure of the filled part of the distribution curve is similar to the structure predicted by Slater. In fact, the low-energy peak of the d-band has been found for all the transition elements studied by the cellular method (21, 28, 22, 23, 29).

A calculation by Fletcher (30) of the density of states for the 3d electrons in nickel gives a width for the filled band of 2.5 ev. This bandwidth is about half that given by Slater. The s-p band is not given in this calculation. The calculation was carried out by the Bloch perturbation method.

The calculated values are summarized in Table IV. The bandwidths of copper and nickel obtained by the cellular method are in satisfactory agreement with the observed bandwidths. The value obtained by the Bloch perturbation method is then too small. The case of iron is peculiar inasmuch as the extrapolation from face-centered copper to body-centered iron, which would not be expected to be reliable, gives better agreement with the observed width than does the value obtained for iron by Manning. The bandwidth of chromium is not in good agreement with the experimental result.

Table IV

Band Emission Data and Theoretical Calculations
(All energies given in electron volts)

	Observed Width	According to Slater	According to Fletcher	According to Manning
Chromium	7.2	3.1		
Manganese	5.8	3.7		
Iron	3.7	4.3		5.0
Nickel	5.8	4.9	2.5	
Copper	7.1	5.5*		

*The width of the s-p band is about 7.3 ev.

The experimental emission edges of copper (Fig. 2), which has a completely occupied d-band, are as sharp as those observed for nickel (Fig. 3), which has a partly filled d-band. If, as we have assumed in the preceding discussion, the experimental emission curves represent only the d-band, we would not expect the characteristic sharp edge at the high-energy side of the copper band. This is one of the observations that suggest that, contrary to our initial assumption, s-like states contribute an appreciable part to the experimental bands. In fact, if we assume that transitions from the s-p band to the $3P_{3/2,\,1/2}$ level have a greater probability than transitions from the five d-bands, we are enabled to give a self-consistent interpretation of a number of features of the experimental bands. It was pointed out to the writer that this is the most plausible assumption to put forward at the present time (31). The copper d- and s-p bands would then be roughly represented as is shown by the dashed line in Fig. 15. We shall return later to the justification for this construction and to the calculated curve shown. First, we shall review some of the expected features of the s-p band. However, we may note that the curve in Fig. 15 portrays, except for the relative height of the s-p and d-bands,

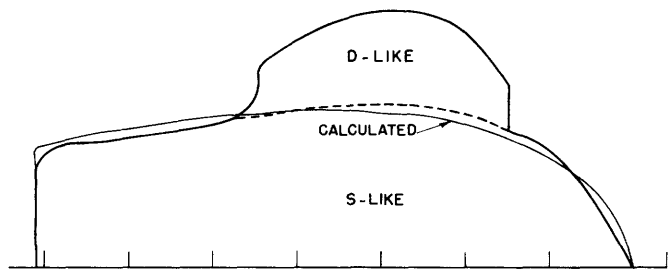

Fig. 15
The electron distribution of copper showing the postulated s-p and d-bands.

the general features predicted for the energy bands of copper – that is, a narrow, filled d-band protruding in the middle of a wider valence band.

The widths of the conduction bands of the metals of the first two periods of the periodic table are given quite accurately by the Sommerfeld free-electron approximation (13, 9). On the basis of calculations of the copper s-p band by Slater (21), Krutter (28), and Fuchs (32), we may expect the same to be true for the transition elements, because, according to these calculations, the electrons in the s-p band behave approximately as free electrons, except in the immediate neighborhood of the nuclei of the ions.

The free-electron theory of metals is based on the assumption that the electronic potential energy is constant in the interior of the metal (33). The energy of an electron in the interior of the metal is then given by

$$E = p^2/2m$$

or

$$E = h^2k^2/2m$$

where p is the electron momentum and k is the wave vector. The density of electrons (in electrons-per-atom-per-unit-energy range) is

$$dN/dE = (4\pi\Omega_o/h^3)\,(2m)^{3/2}\,E^{1/2}$$

The width of the filled band at absolute zero of temperature is

$$E_m = (h^2/2m)\,(3n_o/8\pi\Omega_o)^{2/3}$$

where n_o is the number of free electrons per atom, and Ω_o the atomic volume. We shall neglect temperature effects, since they are too small to be observed with the spectrograph. To be consistent with the number of states filled in the Brillouin zones, the value of E_m should be equal to the energy of free electrons at the surface of the sphere in k space which contains n_o states per atom. To show that this is true in general, at least for metals having face-centered or body-centered-cubic crystal structure, we must find the value of k at the surface of this sphere and use the relation given above to find the energy. The volume of the Brillouin zone is $1/\Omega_o$ (ref. 34), so the volume of the sphere which contains $n_o/2$ of the volume of the zone is $n_o/2\Omega_o$. The value of k at the surface of this sphere is $(3n_o/8\pi\Omega_o)^{1/3}$, corresponding to the energy E_m as we have required. We have made use of the fact that the Brillouin zone for face-centered-cubic and body-centered-cubic crystals contains 2 electrons per atom. It must be remembered that the free electron approximation can only be expected to be valid for n_o less than 1, for it can be shown that near the zone boundary the energy is no longer given simply as a quadratic in k.

In Table V we compare the width of the observed emission bands with the width of the s-p band calculated for free electrons. The number of electrons-per-atom in the s-p bands of nickel, iron, and copper is known from magnetic and conductivity

measurements. For the remainder of the metals the number was arbitrarily taken as 1. The agreement for copper and nickel is good and helps to substantiate the representation of the s-p band shown in Fig. 15. The agreement for iron is not as satisfactory, but the discrepancy could be explained by assuming that the free-electron approximation is not applicable without modification to electrons in the s-p band of iron or that the number of conduction electrons obtained from the magnetic measurements is incorrect. In fact, Seitz (35), to account for the cohesive energy of iron, suggests that half the d-band of iron is not filled, as is assumed to obtain the number of electrons in the s-p band, and that consequently, the number of conduction, or "free," electrons is larger than 0.22. (To facilitate the discussion we are tacitly assuming that the experimental values of the bandwidths are correct.) Since the number of "free" electrons is not known for copper and manganese, we can only state here that interpreting the observed bandwidths of these metals as the width of the s-p band does not lead to any unreasonable conclusions.

Table V

Bandwidths
(All energies in ev)

	Observed	Free Electron	Number of Free Electrons
Chromium	7.2	6.9	1.0 a
Manganese	5.8	6.8	1.0 a
Iron	3.7	2.6	0.22 b
Nickel	5.8	5.3	0.6 b
Copper	7.1	7.1	1.0 b

a – assumed value
b – known value from magnetic and conductivity measurements

We have seen that the width of the observed emission band is approximately equal to the width of the s-p band calculated from the free-electron approximation. Now we want to examine the behavior of electrons in the s-p band more closely in an attempt to predict the shape of the band. As has already been stated, the calculations of the s-p band of copper show that the electrons in this band act approximately as free electrons, except in the immediate neighborhood of the nuclei of the ions. This behavior is similar to that found by Slater (36) for the valence electrons of sodium. Slater found that the energy and the part of the electron wavefunction outside the sodium atom are given with remarkable accuracy by the free-electron approximation. In the neighborhood of the atomic nuclei the wavefunctions have the character of atomic functions. This fact is, of course, the justification for the expansion, given in the beginning of section IV, of the valence-electron wavefunction in atomic wavefunction. By using the notation

introduced in section IV, we may write the density of s-type electrons in the s-p band of copper as

$$(dN/dE)_s^1 = a_s^1 (k)^2 (dN/dE)^1$$

where we have let n = 1 denote the s-p band. Since in the following discussion we shall restrict ourselves to the s-p band, we may drop the superscript. In the light of the preceding discussion we might expect dN/dE to be given with reasonable accuracy by the free-electron approximation. The small energy separation of the atomic 4s and 4p levels suggests that $a_i(k)$ has the same behavior as that already discussed in section IV. Then we have $a_s(k)^2 = 1 - a_p(k)^2$ and $a_p(k)^2 = (k/K_1)^2$ where $k = K_1$ at the edge of the first Brillouin zone. As a result, we may approximate the distribution of s-like electrons in the s-p band by

$$(dN/dE)_s = \left[1 - (k/K_1)^2\right] (dN/dE) = \left[1 - (k/K_1)^2\right] (4\pi\Omega_o/h^3) (2m)^{3/2} E^{1/2}$$

The approximate value of K_1 is given by $\Omega_K = (4\pi K_1^3/3)$, Ω_K being the volume of the zone. We replace k^2 by the corresponding energy given by the free-electron approximation to obtain $(dN/dE)_s$ as a function of energy. To compare this calculated curve with the observed s-p emission band, we must normalize the latter to represent the same number of electrons per atom as the calculated curve. A simple calculation shows that in the case of a half-filled band the calculated curve contains about 5/8 electrons. The calculated and observed curves are compared in Fig. 15. We show the experimental electron distribution separated into the s-p and d-bands. (Part of the s-p band is indicated by the dashed line.) The area under the postulated s-p band is normalized, with the tacit assumption that the transition probability f_{sp} is constant, to represent 5/8 electrons. The agreement between the two curves is remarkably good, considering the crudeness of the assumptions involved. It must be remembered, however, that although the analysis described here helps to give qualitatively the general features of the conduction band, it is definitely incorrect in many details. For example, the electronic specific heat of copper predicted by the free-electron distribution is 0.6×10^{-4} RT compared to the experimental value of 0.89×10^{-4} RT (37), R being the gas constant.

So far, we have only examined the s-p band; we shall now consider the d-band. If the postulated separation of the s-p and d-bands shown in Fig. 15 is correct, the width of the copper d-band is approximately 3 volts. The value obtained by Slater (21) and Krutter (28) is 5.5 ev. The d-band is, however, probably not actually this wide. A later calculation by Chodorow (38) which partially takes into account the exchange effects neglected in the earlier work gives a width of about 4 ev for the copper d-band. This new value obviously is in better agreement with the width of the d-band considered here than with the width obtained by considering the total experimental emission band to represent only the d-band.

We may further check our assumption concerning the postulated d-band by studying the copper 1S emission curve observed by Beeman (3). Beeman attributes most of

his observed intensities to dipole transitions arising from p functions mixed in the s- and d-bands. Superimposed on a broad band of emission due to the s-p band, Beeman obtains a narrow peak that he ascribes to the 3d-band. Beeman then claims that the states giving rise to this radiation are at the top of the 3d-band. With these assumptions, we find that the top of the 3d-band lies about 2.5 ev below the 4s emission edge. This value compares favorably with our value of 2.6 ev (Fig. 15). The distance from the top of the d-band to the Fermi edge is of interest in connection with the color of copper. It has been suggested that the reddish color of copper is due to the ejection of electrons from the 3d-band by the incident light (39). Then, radiation with energy greater than 2.6 ev, which is in the blue region of the visible spectrum, can be strongly absorbed. However, this problem is complicated by transition probabilities, so that we cannot pursue it further.

Since the s-p band calculated for copper fits the experimental data accurately, we would expect that a similar calculation would give the s-p band of nickel. In this case, a comparison of the observed and calculated curves is not possible as there is no natural way to adjust the vertical scale of the observed electron distribution. Fitting the calculated curve to the low-energy part of the nickel curve would not be satisfactory because the exact shape of this part of the band is in doubt. However, since the crystal structures of copper and nickel are the same, the energy bands for the two metals should be similar; except, of course, the d-band of nickel is not filled, and the smaller nuclear charge and smaller lattice spacing might be expected to broaden the bands. We can attempt to separate the nickel d- and s-p bands by analogy to copper as shown in Fig. 16. This procedure would give an experimental width of the d-band of about 3.6 ev which may be compared to 2.5 ev calculated by Fletcher (30) and 4.9 ev calculated by Slater (21). The latter value is probably too large, since it is derived from the copper d-band which Chodorow (38) showed should be contracted by about 1.7 ev.

The postulated separation of the s-p and d-bands shows, except for the relative height of the two bands, the general features predicted from the observed properties of nickel. The narrow unfilled d-band is required to explain the ferromagnetic behavior

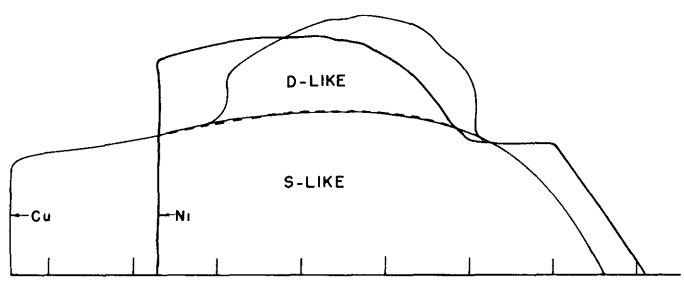

Fig. 16
The electron distribution of copper and nickel showing the postulated s-p and d-bands.

and the high electronic specific heat observed. The electronic specific heat is proportional to the density of electrons at the Fermi edge. As we have seen in the beginning of this section, the density of electrons in the d-band is much greater than the density of electrons in the conduction band. Consequently, we may, in general, expect metals with unfilled d-bands to have a large electronic specific heat. For example, the electronic specific heat of nickel is 8.72×10^{-4} RT (40), about 10 times larger than the electronic specific heat of copper. If we normalize the postulated nickel d-band, shown in Fig. 16, to represent 9.4 electrons, we can obtain a numerical value for the density of electrons at the Fermi edge. We then obtain for the electronic specific heat, 8.5×10^{-4} RT which is in good agreement with the measured value given above. The contribution of the s-p band to the density of electrons at the Fermi edge has been neglected, as it is an order of magnitude smaller than the contribution of the d-band. These results are of course only qualitative, since we have neglected any possible admixture of p-type electrons in the d-band and any variation of the transition probability, but they show that the shape of the postulated d-band is consistent with the observed electronic specific heat.

The s-p bands of iron, chromium, and manganese might also be expected to be similar to the one calculated for copper, even though the crystal structure of these metals is different. In order to make a comparison of the observed and calculated curves possible, we must adjust the vertical scale of the observed curves. As in the case of nickel, there is no unique way to do this. Furthermore, a comparison with the copper emission curve can no longer be expected to be valid. Therefore, we arbitrarily adjust the observed manganese curve to fit the calculated s-p band at 2.5 ev (Fig. 17). This procedure results in fair agreement of the low-energy parts of the observed and calculated curves. With less justification, the parabolic rise of the calculated curve is fitted to the bottom of the observed chromium band (Fig. 18). Although these separations of the observed electron distributions into the d- and s-p bands are somewhat arbitrary, they form a basis for a discussion of the energy bands. The manganese curve has the expected behavior, a narrow unfilled d-band and a wider conduction band. The d-band is about 3.0 ev wide. The unfilled d-band of manganese would indicate a large electronic specific heat, but certainly not as large as the observed value of 21×10^{-4} RT (41), 2.5 times larger than that of nickel. The calculated s-p band of chromium, shown in Fig. 18, obviously is not correct, since it requires that the d-band be filled. However, the low-electronic specific heat of chromium indicates

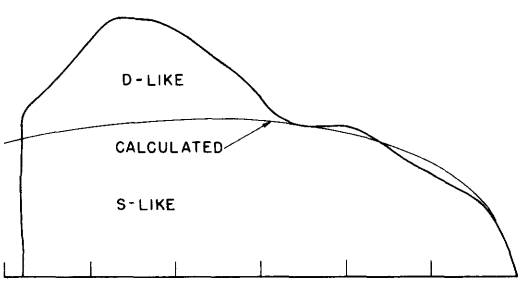

Fig. 17
The electron distribution of manganese showing the postulated s-p and d-bands.

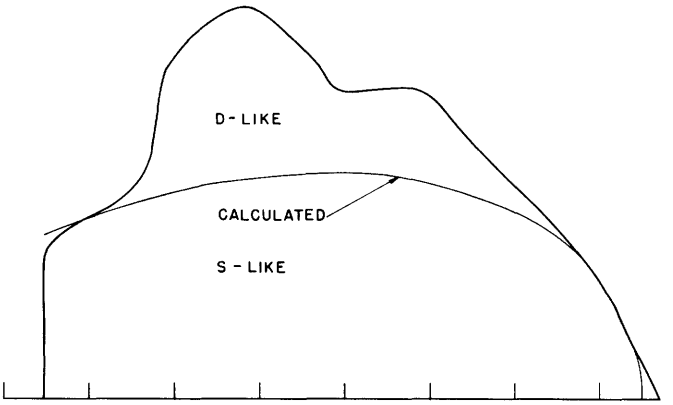

Fig. 18
The electron distribution of chromium showing the postulated s-p and d-bands.

that the general features of the separation of the s-p and d-bands may be correct. The measured value of the electronic specific heat of chromium is 1.9×10^{-4} RT (42), only about 2 times larger than that expected from the s-p band alone. The postulated d-band, which appears to drop to a low intensity at the emission edge, is consistent with the expected low density of states at the Fermi edge. The low-energy limit of the chromium d-band is not clearly marked, except perhaps by the inflection in the band, 3.4 ev below the emission edge. The latter interpretation does not, however, fit the calculated s-p band shown, but since the separation of the d- and s-p bands of chromium has less justification than the postulated separations discussed for the other metals, we shall not pursue this topic further. We shall not attempt to separate the iron s-p and d-bands, since the accuracy of the experimental curves is too low to give us much confidence in the results. However, a comparison of the iron curve (Fig. 18) and the nickel curve (Fig. 16) shows that we might say that the d-band of iron is about 2.2 ev wide. If this value is correct, the d-band of iron is about half as wide as was calculated by Manning (22). This analysis of the iron band will, of course, only be valid if our assumptions concerning the relative intensities of the s-p and d-bands are correct.

VI. Conclusion

We have seen that, at least for copper and nickel, a plausible explanation of the observed bands can be obtained with the assumption that the s-p band produces an appreciable part of the observed intensity. In order to carry this analysis further from an experimental viewpoint, it would be necessary to obtain a more reliable iron emission curve and the absorption curve of copper. If the observed copper emission band reflects the density of only d electrons, the copper absorption edge would appear at a higher energy than the high-energy limit of the observed emission bands. If the sharp rise at the high-energy side of the experimental copper curve is really the Fermi edge,

the absorption and emission edges would, of course, coincide. To eliminate any uncertainty in the position of the edges, the emission and absorption curves should be obtained with the same spectrograph. The higher sensitivity of the photomultiplier should make it possible to use the continuous x-ray spectrum as a source for the absorption experiments. These experiments would require extensive modifications of the spectrograph used in the work described here, or the construction of a new instrument. Experience with the present spectrograph indicates that to obtain a more satisfactory iron curve a better vacuum must be maintained. Consequently, a new spectrograph should probably have a glass specimen chamber arranged so that the chamber can be baked to outgas the walls. A multiple-slit system in conjunction with differential pumping would be required to isolate the glass specimen chamber from the metal parts of the spectrograph.

Acknowledgment

The work described here would not have been possible without the early forethought and guidance of Dr. E. R. Piore, who initiated the soft x-ray emission project while on leave of absence from the Office of Naval Research. Much valuable experience was gained by working with Dr. R. H. Kingston, who first used the spectrograph. It is to Professor G. G. Harvey, who supervised the project, that the writer is especially indebted for continued interest, valuable discussion, and encouragement. I am grateful to Dr. R. H. Parmenter of the Solid State and Molecular Theory Group for many clarifying discussions. And finally, I wish to express appreciation for receiving a fellowship grant made possible by the International Business Machines Corporation.

References

1. J. A. Bearden, W. W. Beeman: Phys. Rev. 58, 387, 1940
2. J. A. Bearden, W. W. Beeman: Phys. Rev. 58, 396, 1940
3. W. W. Beeman, H. Friedman: Phys. Rev. 58, 400, 1940
4. E. Saur: Z. Physik 103, 421, 1936
5. H. Gwinner: Z. Physik 108, 523, 1938
6. J. Farineau: Nature 140, 508, 1937
7. H. W. B. Skinner, J. E. Johnston: Nature 140, 508, 1937

8. E. R. Piore, G. G. Harvey, E. M. Gyorgy, R. H. Kingston: Rev. Sci. Instr. 23, 8, 1952
9. R. H. Kingston: Phys. Rev. 84, 944, 1951
10. W. Heitler: The Quantum Theory of Radiation, p. 110, Oxford, 1944
11. H. W. B. Skinner, J. E. Johnston: Proc. Roy. Soc. (London) A161, 420, 1937
12. N. C. Pearson: Bachelor's Thesis, Department of Physics, M.I.T., 1952
13. H. W. B. Skinner: Trans. Roy. Soc. (London) A239, 95, 1940
14. H. Niehrs: Ergeb. exakt. Naturwiss. 23, 359, 1950
15. M. Siegbahn: Spektroskopie der Röntgenstrahlen, Verlag Julius Springer, Berlin, 1931
16. R. Coster, R. De L. Kronig: Physica 2, 13, 1935
17. H. W. B. Skinner: Reports on Progress in Physics V, 257, Phys. Soc. London, England, 1939
18. N. F. Mott, H. Jones, H. W. B. Skinner: Phys. Rev. 45, 379, 1934
19. J. C. Slater: Quantum Theory of Matter, p. 146, McGraw-Hill, New York, 1951
20. H. M. Krutter: Phys. Rev. 48, 664, 1935
21. J. C. Slater: Phys. Rev. 49, 537, 1936
22. M. F. Manning: Phys. Rev. 63, 190, 1943
23. J. B. Greene, M. F. Manning: Phys. Rev. 63, 203, 1943
24. F. Seitz: Modern Theory of Solids, p. 436, McGraw-Hill, New York, 1940
25. J. C. Slater: Phys. Rev. 76, 1592, 1949
26. N. F. Mott: Proc. Phys. Soc. (London) 47, 571, 1935
27. E. Rudberg, J. C. Slater: Phys. Rev. 50, 150, 1936
28. H. M. Krutter: Phys. Rev. 48, 664, 1935
29. M. F. Manning, M. I. Chodorow: Phys. Rev. 56, 787, 1939
30. G. C. Fletcher: Proc. Roy. Soc. (London) A65, 192, 1952
31. F. Seitz: Private communication
32. K. Fuchs: Proc. Roy. Soc. (London) A151, 585, 1935
33. F. Seitz: Modern Theory of Solids, chap. IV, McGraw-Hill, New York, 1940
34. N. F. Mott, H. Jones: Properties of Metals and Alloys, p. 158, Oxford, 1936
35. F. Seitz: Modern Theory of Solids, p. 430, McGraw-Hill, New York, 1940
36. J. C. Slater: Phys. Rev. 45, 794, 1934
37. J. A. Kok, W. H. Keesom: Physica 3, 1035, 1936
38. M. Chodorow: Phys. Rev. 55, 675A, 1939
39. F. Seitz: Modern Theory of Solids, p. 424, McGraw-Hill, New York, 1940
40. W. H. Keesom, C. W. Clark: Physica 2, 513, 1935
41. Elson, Grayson-Smith, Wilhelm: Can. J. Res. 18, 82, 1940
42. I. Estermann, S. A. Friedberg, J. E. Goldman: Phys. Rev. 87, 582, 1952